THE JOURNAL OF BIOLOGICAL CHEMISTRY VOL. 280, NO. 39, pp. 33338–33345, September 30, 2005

Both Rotor and Stator Subunits Are Necessary for Efficient Binding of F_1 to F_0 in Functionally Assembled *Escherichia coli* ATP Synthase*

Received for publication, June 8, 2005, and in revised form, July 27, 2005 Published, JBC Papers in Press, August 5, 2005, DOI 10.1074/jbc.M506251200

Thomas Krebstakies[‡1,2], **Boris Zimmermann**[§1,3], **Peter Gräber**[§], **Karlheinz Altendorf**[‡], **Michael Börsch**[¶3,4], **and Jörg-Christian Greie**[‡5]

From the [‡]*Fachbereich Biologie/Chemie, Abteilung Mikrobiologie, Universität Osnabrück, D-49069 Osnabrück, Germany, the* [§]*Institut für Physikalische Chemie, Universität Freiburg, Albertstrasse 23a, D-79104 Freiburg, Germany, and the* [¶]*Physikalisches Institut, Universität Stuttgart, Pfaffenwaldring 57, D-70569 Stuttgart, Germany*

In F_1F_0-ATP synthase, the subunit $b_2\delta$ complex comprises the peripheral stator bound to subunit *a* in F_0 and to the $\alpha_3\beta_3$ hexamer of F_1. During catalysis, ATP turnover is coupled via an elastic rotary mechanism to proton translocation. Thus, the stator has to withstand the generated rotor torque, which implies tight interactions of the stator and rotor subunits. To quantitatively characterize the contribution of the F_0 subunits to the binding of F_1 within the assembled holoenzyme, the isolated subunit *b* dimer, ab_2 subcomplex, and fully assembled F_0 complex were specifically labeled with tetramethylrhodamine-5-maleimide at *b*Cys[64] and functionally reconstituted into liposomes. Proteoliposomes were then titrated with increasing amounts of Cy5-maleimide-labeled F_1 (at γCys[106]) and analyzed by single-molecule fluorescence resonance energy transfer. The data revealed F_1 dissociation constants of 2.7 nM for the binding of F_0 and 9–10 nM for both the ab_2 subcomplex and subunit *b* dimer. This indicates that both rotor and stator components of F_0 contribute to F_1 binding affinity in the assembled holoenzyme. The subunit *c* ring plays a crucial role in the binding of F_1 to F_0, whereas subunit *a* does not contribute significantly.

F-type ATPases (F_1F_0) are ubiquitously abundant in the inner membranes of mitochondria, chloroplasts, and bacteria, where they catalyze the synthesis of ATP by oxidative or photophosphorylation. In bacteria, the enzyme can also work in the opposite direction to generate proton or sodium gradients at the expense of ATP. Despite slight variations in subunit composition among species, F_1F_0 complexes share a high homology with respect to the mechanism of catalysis, in which ion translocation through the membrane-embedded F_0 part is rotationally coupled to ATP synthesis/hydrolysis in F_1 (1). Because of the rotary mechanics, in addition to the structural classification of this multisubunit enzyme complex in F_1 (subunit composition $\alpha_3\beta_3\gamma\delta\epsilon$ in *Escherichia coli*) and F_0 (ab_2c_{10}) (2), a functional classification into rotor and stator is also used. Either H^+ translocation through F_0 or ATP hydrolysis in F_1 leads to the rotary movement of a centrally located $\gamma\epsilon c_{10}$ rotor element (3–8), which has to be counteracted by a peripheral stator element. This so-called "second stalk" is composed at least of the two copies of subunit *b* (9, 10), which are supposed to undergo transient elastic deformation to compensate for the torque, which is built up by the propelling rotor (5, 11, 12). Accordingly, a similar mode of elastic coupling during catalysis has recently been suggested for the subunit *c* ring of the rotor part from the Na^+-translocating ATP synthase of *Ilyobacter tartaricus* (13).

The peripheral connection between F_1 and F_0 by subunit *b* is accomplished by multiple contacts of the subunit *b* dimer with the α, β, and δ subunits of F_1 (10, 14, 15) as well as with subunit *a* of F_0 (16–18). Because of the transient storage of elastic energy during catalysis, subunit interactions between components of the stator have to be rather strong to withstand a rotary strain of up to 55 kJ mol^{-1}, *i.e.* the maximum ΔG observed for ATP synthesis (19, 20). Although there are several binding partners for subunit *b* within the stator in F_1, each of which contributes to binding affinity (21, 22), in the case of F_0, only subunit *a* interacts with the subunit *b* dimer. Although binding affinities between subunits *a* and *b* could so far not be determined within the lipid phase, a strong interaction has been shown by the purification of a stable ab_2 subcomplex (23). In the case of the interaction of subunit *b* with F_1, binding affinities have so far been determined only in solution by several techniques, including fluorometric tryptophan quenching (1, 22, 24) and fluorescence resonance energy transfer (FRET)[6] (20). However, in these assays, only truncated forms of subunit *b* lacking the membrane part were used, thereby confusing the interpretation of the corresponding results with a rather weak dissociation constant for dimerization (20, 22). Subunit *b* dimerization was shown to be a prerequisite for F_1 binding (25), and the two copies of subunit *b* were shown to interact also within the transmembrane portion of the polypeptide (26). In addition, the use of soluble F_1 and single F_0 subunits in titration assays does not allow testing of functional F_1/F_0 interactions because of the lack of the membrane-embedded F_0 part of the enzyme. It has previously been shown that, in the case of reconstituted F_0 and its subcomplexes, all three subunits *a*, *b*, and *c* are necessary for the functional binding of F_1 (11, 23, 27). Thus, both rotor (subunit *c*) and stator (subunit *b*) components of F_0 contribute to F_1 binding *in vivo*.

In this study, F_1/F_0 interactions were quantified for the first time using functionally reconstituted protein complexes. The binding of F_1 to the subunit *b* dimer and ab_2 stator subcomplexes as well as to fully assembled F_0 has been observed by single-molecule FRET, also introducing a new approach in the spectroscopic analysis of binding constants in F_1/F_0 interaction. The binding constants clearly demonstrate

* This work was supported in part by Deutsche Forschungsgemeinschaft Grant SFB431/P2. The costs of publication of this article were defrayed in part by the payment of page charges. This article must therefore be hereby marked "*advertisement*" in accordance with 18 U.S.C. Section 1734 solely to indicate this fact.

[1] Both authors contributed equally to this work.

[2] Supported by a fellowship from the Fonds der Chemischen Industrie.

[3] Supported by Landesstiftung Baden-Württemberg Project "Functional Nanodevices."

[4] To whom correspondence may be addressed. Tel.: 49-711-685-4632; Fax: 49-711-685-5281; E-mail: m.boersch@physik.uni-stuttgart.de.

[5] To whom correspondence may be addressed. Tel.: 49-541-969-2809; Fax: 49-541-969-2870; E-mail: greie@biologie.uni-osnabrueck.de.

[6] The abbreviations used are: FRET, fluorescence resonance energy transfer; DDM, *n*-dodecyl β-D-maltoside; TMR, tetramethylrhodamine-5-maleimide; MOPS, 4-morpholinepropanesulfonic acid; Tricine, *N*-[2-hydroxy-1,1-bis(hydroxymethyl)ethyl]glycine; FCS, fluorescence correlation spectroscopy.

that both rotor and stator components of F_0 contribute to F_1 binding affinity in the assembled holoenzyme.

EXPERIMENTAL PROCEDURES

Construction of Plasmids and Growth Conditions—Plasmid pTOM3.1 was constructed by cloning a 144-bp EcoNI fragment from pSK1 (28) as well as a 478-bp PpuMI/BssHI fragment from pRR76 (29) into plasmid pBWU13 (*atpI′BEFHAGDC*) (30), thereby introducing the substitutions *b*C21A and *b*Q64C. Addition of a polyhistidine motif following the N-terminal methionine residue of subunit *a* was achieved by the site-directed introduction of a $(CATCAC)_6$ sequence via a two-stage PCR mutagenesis procedure (31), yielding plasmid pTOM3.1*a*His_{12}. Both plasmids were transformed into *E. coli* strain DK8 (Δ*atpBEFHAGDC*) (32), and cultures were grown on minimal medium with glycerol as the carbon source (11). Cells were harvested at late exponential phase and stored at −80 °C.

Preparative Methods—The preparation of F_1 from *E. coli* RA1/pRA114 (33, 34) containing the mutation γT106C was carried out as described (33). F_0 and subunit *b* from DK8/pTOM3.1 were isolated as described previously (11, 35). To purify the ab_2 subcomplex, everted membrane vesicles were prepared at 4 °C by resuspending 50 g of DK8/pTOM3.1*a*His_{12} cells in 50 mM Tris-HCl (pH 8.0), 10 mM $MgCl_2$, and 10 μg/ml DNase, followed by cell disruption with a Constant Systems Basic Z cell disrupter (IUL Instruments GmbH) at a pressure of 1.36 kilobars. The membrane suspension was centrifuged at 15,000 × *g* for 30 min. To separate everted membrane vesicles from the cytosolic fraction, the supernatant was centrifuged at 150,000 × *g* for 1.5 h. To remove F_1, membranes were washed with 10 mM Tris-HCl (pH 7.5), 10 mM EDTA, and 10% (v/v) glycerol; resuspended in 1 mM Tris-HCl (pH 7.5), 6 M urea, and 10% (v/v) glycerol; and incubated overnight. Membranes were collected by centrifugation and washed with 50 mM Tris-HCl (pH 7.5) and 10% (v/v) glycerol. For solubilization, membranes (10 mg/ml) were stirred with 1.4% (w/v) *n*-dodecyl β-D-maltoside (DDM) (Glycon Corp.) at 4 °C for 1 h and subsequently centrifuged at 232,000 × *g* for 15 min. The supernatant was adjusted to 150 mM NaCl, 10 mM imidazole, and 0.1 mM phenylmethylsulfonyl fluoride and incubated with 1 ml of nickel-nitrilotriacetic acid-agarose (Qiagen Inc.)/10 mg of membrane protein at 4 °C for 1 h. The agarose matrix was pre-equilibrated with 50 mM Tris-HCl (pH 7.5), 10% (v/v) glycerol, 150 mM NaCl, 10 mM imidazole, 0.05% (w/v) DDM, and 0.1 mM phenylmethylsulfonyl fluoride. The agarose was then packed into an empty glass column and washed with 5–10 column volumes of the equilibration buffer. To remove unspecifically bound protein, the imidazole concentration was temporarily increased to 60 mM for 5–10 column volumes, followed by a decrease to 10 mM for another 5–10 column volumes. Detergent was exchanged from DDM to Na^+ cholate using 5–10 column volumes of the equilibration buffer containing 1% (w/v) Na^+ cholate instead of DDM. Elution of the ab_2 subcomplex with 250 mM imidazole was preceded by a gradient from 10 to 55 mM imidazole within 10 column volumes. Eluted protein was concentrated to 0.5–1 mg/ml using Amicon Ultra-4 centrifugal filter devices (molecular weight cutoff of 10,000; Millipore Corp.) and dialyzed against a 1000-fold volume of 50 mM Tris-HCl (pH 7.5), 10% (v/v) glycerol, 150 mM NaCl, 10 mM imidazole, 1% (w/v) Na^+ cholate, and 0.1 mM phenylmethylsulfonyl fluoride for 24 h with changing the buffer once.

Labeling F_0 Components and F_1—Isolated F_0, subunit *b*, and ab_2 subcomplex were labeled with tetramethylrhodamine-5-maleimide (TMR) (Molecular Probes, Inc.), whereas purified F_1 was labeled with Cy5-maleimide (referred to as Cy5; Amersham Biosciences). The dyes were initially dissolved in dimethyl sulfoxide, and their concentrations were determined after a 1000-fold dilution with methanol using the extinction coefficients provided by the supplier. The Förster radius (R_0) for this FRET pair is ~6.4 nm (7).

F_0 and subcomplexes thereof were labeled at *b*Cys^{64} with TMR in 10 mM Tris/NaOH (pH 8.0), 150 mM NaCl, 1% (w/v) Na^+ cholate, and 10% (v/v) glycerol on ice in the presence of a 5-fold excess of tris(2-carboxyethyl)phosphine hydrochloride (Molecular Probes, Inc.) with respect to protein to prevent the formation of disulfides. To avoid the labeling of both *b* subunits within the dimer, the degree of labeling was adjusted to ~35% by applying the fluorescent dye at different molar ratios and incubation times, *i.e.* for F_0, a molar ratio of 1:1 for 3 h; for the ab_2 subcomplex, a molar ratio of 1:5 for 4.5 h; and for subunit *b*, a molar ratio of 1:5 for 1.5 h. In the latter case, 50 mM MOPS (pH 7.0), 100 mM NaCl, 100 μM $MgCl_2$, and 0.1% (w/v) DDM was used. Unbound dye and tris(2-carboxyethyl)phosphine hydrochloride were removed using pre-equilibrated Sephadex G-50 columns (Amersham Biosciences). The labeling degrees (β) were calculated from the concentration ratio of bound dye and protein according to the following: $\beta = ([\text{labeled protein}]/[\text{total protein}]) \times 100\% = ((A_{556}/\epsilon_{556(TMR)})/(A_{278(protein)}/\epsilon_{278(protein)})) \times 100\%$ and $A_{278(protein)} = A_{278(total)} - A_{278(TMR)} = (A_{278(total)} - (\epsilon_{278(TMR)}/\epsilon_{556(TMR)}) \times A_{556}$, where A_{278} and A_{556} are the absorbance at 278 and 556 nm, respectively; and ϵ_{278} and ϵ_{556} are the extinction coefficients at 278 and 556 nm, respectively. The concentrations were determined from UV-visible absorption spectra of the labeled proteins using $\epsilon_{278(F_0)} = 136{,}000\ M^{-1}\ cm^{-1}$, $\epsilon_{278(ab_2)} = 108{,}000\ M^{-1}\ cm^{-1}$, $\epsilon_{278(TMR)} = 19{,}500\ M^{-1}\ cm^{-1}$, and $\epsilon_{556(TMR)} = 95{,}000\ M^{-1}\ cm^{-1}$, yielding TMR labeling rates of 32% for F_0 and 36% for the ab_2 subcomplex. The rather low absorbance of subunit *b* ($\epsilon_{278} = 7100\ M^{-1}\ cm^{-1}$) was masked by the absorbance of TMR itself. Thus, for TMR-labeled subunit *b*, the protein concentration was determined with the enhanced BCA protein assay (Pierce) using unlabeled subunit *b* as a standard. The TMR concentration was then measured by UV-visible spectroscopic absorption analysis, from which a labeling degree of 29% was calculated.

F_1 was labeled at γCys^{106} with Cy5 at a molar ratio of 1:0.9 in 50 mM MOPS/NaOH (pH 7.0) and 100 μM $MgCl_2$ on ice for 4 min (36). Unbound dye was removed by gel filtration on Sephadex G-50. A labeling degree (α) of ~58% was calculated from UV-visible absorption spectra (for details, see above) using $\epsilon_{650(Cy5)} = 250{,}000\ M^{-1}\ cm^{-1}$, $\epsilon_{278(Cy5)} = 41{,}100\ M^{-1}\ cm^{-1}$, and $\epsilon_{278(F_1)} = 205{,}500\ M^{-1}\ cm^{-1}$. Solutions of labeled protein were frozen in liquid nitrogen after addition of 10% (v/v) glycerol and stored at −80 °C.

Reconstitution of F_0, the ab_2 Subcomplex, and Subunit b into Liposomes and Reassembly with F_1—Liposomes from phosphatidylcholine and phosphatidic acid were prepared by dialysis (37). TMR-labeled F_0, ab_2 subcomplex, and subunit *b* were reconstituted according to Fischer *et al.* (38). The final concentration of proteoliposomes was 8 mg/ml of lipid in 20 mM Tricine/NaOH (pH 8.0), 20 mM succinate, 2.5 mM $MgCl_2$, and 0.6 mM KOH. For the determination of catalytic activities and ensemble fluorescence measurements, the enzyme concentration was adjusted to 40 nM. In the case of single-molecule fluorescence measurements, the concentration of reconstituted protein was 15 nM, resulting in an average number of less than one enzyme molecule/liposome (8). Proteoliposomes were incubated with different concentrations of labeled F_1 (0, 0.09, 0.9, 9, 49, 89, 222, and 444 nM) in the presence of 2.5 mM $MgCl_2$ and 50 mM NaCl for 45 min at 37 °C, followed by a 90-min incubation on ice. Unbound F_1 was removed by subsequent centrifugation at 265,000 × *g* for 90 min, and the pellet was resuspended in 20 mM Tricine/NaOH (pH 8.0), 20 mM succinate, 0.6 mM KCl, 2.5 mM $MgCl_2$, and 4% (v/v) glycerol.

Fluorescence Measurements—Ensemble fluorescence measurements were performed at 20 °C using an SLM-AMINCO 8100 spectrofluorometer with a slit width of 4 nm. Spectra were corrected for lamp intensity and detection efficiency.

Single-molecule fluorescence measurements were performed at 20 °C using a confocal microscope (100-μm pinhole size) of local design. The laser beam (532 nm, frequency-doubled neodymium/yttrium aluminum garnet; Coherent Inc.) was attenuated to 100 microwatts and directed into an Olympus water immersion objective (UApo 40×, numerical aperture of 1.15). This power level created sufficiently high fluorescence signals, but still kept photobleaching negligible. For epi-illumination, a 545 nm DCLP dichroic mirror (AHF Corp.) was used. Fluorescence was subdivided by a 630 nm DCLP dichroic mirror into two spectral ranges with $\lambda < 630$ nm for TMR and $\lambda > 630$ nm for Cy5 and detected with two avalanche photodiodes (SPCM-AQR 151, EG&G). Filters (HQ 575/65 nm for TMR and HQ 665 nm LP for Cy5) were used to block laser light scattering and to reduce the cross-talk of TMR into the Cy5 detection channel to 5.4%. The excitation efficiency of Cy5 at 532 nm was <0.03 times that of TMR. Photons were recorded simultaneously (1-ms time resolution) with a multiscaler photon counter (PMS-300, Becker & Hickl GmbH). Samples were analyzed on a microscope slide with a cavity of ~85 μl covered with a cover glass. Labeled proteoliposomes were diluted to a final concentration of ~100 pM in 20 mM Tricine/NaOH (pH 8.0), 20 mM succinate, 0.6 mM KCl, and 2.5 mM $MgCl_2$. At this concentration, one liposome at most was present in the confocal volume at the same time.

For fluorescence correlation spectroscopy (FCS), only the photons of the TMR channel were used to calculate the autocorrelation function ($G(\tau_c)$) by an ALV 5000/E FAST real-time correlator. For a quantitative interpretation, we used the following function, which contains a diffusion term and a contribution of one triplet state (Equation 1),

$$G(\tau_c) = 1 + \frac{1}{N_F}\left(\frac{1}{1 + \tau_c/\tau_D}\right) \cdot \left(\frac{1}{1 + (\omega_0/z_0)^2\tau_c/\tau_D}\right)^{1/2} \cdot (1 - T + T^{(-\tau_c/\tau_T)}) \quad \text{(Eq. 1)}$$

where $G(\tau_c)$ is the autocorrelation function; N_F is the average number of fluorescent molecules in the detection volume; τ_c is the correlation time; $\tau_D = \omega_0^2/4D$ is the characteristic time of diffusion with D (diffusion coefficient); τ_T is the characteristic triplet time; T is the average fraction of molecules in the excited triplet state; and ω_0 and z_0 are the $1/e_2$ radii of the gaussian detection volume in the radial and axial directions, respectively. The actual confocal detection volume (V = 7.7 fl) was calculated from the FCS data of rhodamine 6G in water as described (36). For FCS, samples were diluted to a final concentration of 2–5 nM, which yielded a mean value of 5–10 molecules within the confocal volume at the same time. For every single-molecule FRET titration experiment, three independent measurements were performed. To determine the diffusion times (τ_D), the autocorrelation functions were fitted by Equation 1. All best fits of FCS data resulted in similar values for the triplet contribution, *i.e.* τ_T (4 μs) and T (0.03–0.07).

Determination of K_d by Single-molecule FRET Analysis—Single-molecule FRET data were analyzed by the custom-made software Burst Analyzer. After correction of background count rates (0.5–2 counts/ms) and cross-talk of TMR into the Cy5 channel, photon bursts were selected by the following criteria. 1) A duration time of >20 ms identified photon bursts originating from labeled proteoliposomes with a corresponding mean diffusion time through the confocal detection volume. 2) Count rates higher than 10 photons/ms for the TMR channel or higher than seven photons/ms for the Cy5 channel enabled the unambiguous determination of the presence of both fluorophores in the proteoliposome. 3) Photon bursts were excluded from further analysis if the total count rate, *i.e.* the sum of photons in the donor and acceptor channels, was >7000 because these bursts presumably indicate aggregates of liposomes.

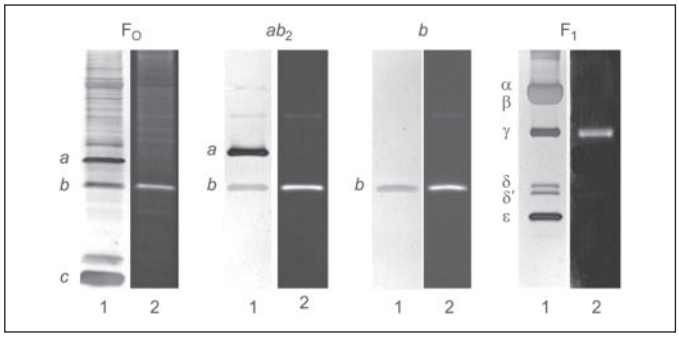

FIGURE 1. **SDS-PAGE of labeled F_1 and F_0 and its subcomplexes.** F_0, subunit *b*, and the ab_2 subcomplex were labeled at *b*Cys[64] with TMR, and F_1 was labeled at γCys[106] with Cy5. 5 μg of F_1 and F_0 as well as corresponding stoichiometric amounts of subunit *b* and the ab_2 subcomplex were used for SDS-PAGE. Before the gel was silver-stained (*lanes 1*), it was documented under UV light (*lanes 2*). The apparent difference in the concentration of subunit *a* compared with subunit *b* is due to stronger staining of subunit *a*. The additional histidine residues of the His_{12} tag-modified ab_2 subcomplex are responsible for the increased molecular mass of subunit *a*. The partial degradation of the δ subunit in purified F_1 is indicated (δ').

For each selected burst, the apparent mean FRET efficiency was calculated by $E_{app} = I_A/(I_A + I_D)$, with I_A and I_D being the corrected intensities of Cy5 (acceptor) and TMR (donor), respectively. Bursts were classified as either donor-only events ($E_{app} \leq 0.05$) or FRET events ($E_{app} > 0.05$), and the ratio of FRET events to all events was calculated and plotted against the F_1 concentration.

Assays—Protein concentrations were determined either by the BCA assay used as recommended by the supplier or by UV absorption spectroscopy using the extinction coefficients given above (39). Proteins were separated by SDS-PAGE (16.5% T and 6% C separating gels together with 4% T and 3% C stacking gels) (40) and detected by silver staining (41). Specificity of subunit labeling was controlled by fluorescence detection of protein bands. ATPase activities were measured in an ATP-regenerating system (42) at 37 °C in 100 mM Tris-HCl (pH 8.0), 25 mM KCl, 4 mM $MgCl_2$, 2.5 mM phosphoenolpyruvate, 18 units/ml pyruvate kinase, 16 units/ml lactate dehydrogenase, and 0.2 mM NADH. ATP synthesis was measured after an acid-base transition in the presence of an additional K^+/valinomycin diffusion potential at room temperature (43). 20 μl of F_1F_0 liposomes (40 nM) were incubated for 3 min with 80 μl of 20 mM succinate/NaOH (pH 4.7), 5 mM NaH_2PO_4, 0.6 mM KOH, 2.5 mM $MgCl_2$, 100 μM ADP, and 20 μM valinomycin. 100 μl of the acidified suspension were then mixed with 900 μl of 200 mM Tricine/NaOH (pH 8.8), 5 mM NaH_2PO_4, 160 mM KOH, 2.5 mM $MgCl_2$, and 100 μM ADP. The formation of ATP was monitored with a luciferin/luciferase assay.

RESULTS

Purification and Fluorescence Labeling of Proteins—To observe binding of F_1 to F_0 and components thereof by intramolecular FRET, it was necessary to specifically label one subunit of each of the binding partners. All subunits were isolated and labeled with TMR (F_0, ab_2 subcomplex, and subunit *b*) or with Cy5 (F_1) as described under "Experimental Procedures" (Fig. 1). Labeling degrees were determined by UV-visible absorption spectroscopy as described under "Experimental Procedures" and calculated to be 29–36% for TMR-labeled *b*Cys[64] in F_0, the ab_2 subcomplex, and subunit *b* and 58% for Cy5-labeled F_1 γCys[106]. For the ab_2 subcomplex and subunit *b*, UV illumination of the SDS gel revealed an additional slightly fluorescent protein band corresponding to the subunit *b* dimer. In the case of F_0, the remaining impurities did not superimpose on the fluorescence of TMR at *b*Cys[64], which was required

TABLE ONE

Rates of ATP synthesis and hydrolysis catalyzed by labeled F_1F_0 and F_1, respectively

Isolated F_0 bCys[64] (40 nM) was reconstituted into liposomes, and the rates of ATP synthesis were measured at 20 °C after rebinding F_1 γCys[106] and energization by Δ pH and $\Delta\phi$. ATP hydrolysis (10 nM F_1 γCys[106]) was measured with an ATP-regenerating system at 37 °C. Values are the means ± S.D. from duplicate measurements. F_1 and F_0 were labeled as indicated: F_1^{Cy5}, Cy5-labeled F_1; F_0^{TMR}, TMR-labeled F_0.

Compound/conditions	Turnover
	s^{-1}
ATP synthesis	
F_1F_0	14 ± 2
$F_1^{Cy5}F_0$	16 ± 7
$F_1F_0^{TMR}$	15 ± 5
$F_1^{Cy5}F_0^{TMR}$	14 ± 3
ATP hydrolysis	
F_1	121 ± 9
F_1^{Cy5}	123 ± 6

for the FRET analysis. γCys[106] of purified F_1 showed highly specific labeling with Cy5. The silver-stained SDS gel also revealed partial degradation of subunit δ, which has already been observed as a common problem in F_1 preparations (44).

Functionality of Labeled Proteins—Previous studies revealed the functionality of isolated F_0, ab_2 subcomplex, and subunit b by passive proton translocation through F_0 reconstituted from subcomplexes as well as from single subunits (11, 23, 27). To exclude a possible influence of the dye on the catalytic function of F_1 and the coupling to F_0, the rates of ATP synthesis and hydrolysis were determined with both the labeled and unlabeled enzymes. Isolated F_0 was reconstituted into liposomes; and after binding of F_1, all samples revealed nearly the same rate of ATP synthesis of ~15 s^{-1} (TABLE ONE). Accordingly, ATP hydrolysis turnover rates of ~120 s^{-1} were determined for isolated F_1, whether Cy5-labeled or not. Both assays clearly demonstrate that the functionality of F_1 and F_0 was not affected by the labeling procedure.

Analysis of Ensemble Fluorescence Spectra—The basic concept of the FRET assay is as follows. Excitation of the fluorescent donor attached to F_0, the ab_2 subcomplex, or subunit b results in an energy transfer to the fluorescent acceptor only after binding of an acceptor-labeled F_1 complex. According to the theory of FRET (45), this energy transfer depends on the distance between both fluorophores and their spectroscopic properties. The spectroscopic properties of the TMR-labeled F_0 complex and F_0 components (FRET donors) incorporated into liposomes and Cy5-labeled F_1 (FRET acceptor) are shown in Fig. 2. To circumvent light scattering caused by the proteoliposomes, fluorescence excitation spectra were measured instead of absorbance spectra. The fluorescence excitation (*curves 1*) and fluorescence emission (*curves 2*) spectra of reconstituted and TMR-labeled F_0, ab_2 subcomplex, and subunit b were identical, which was also found for the corresponding samples in buffer solution (data not shown). This clearly demonstrates that the protein composition and/or environment had no influence on the TMR fluorescence. The fluorescence excitation spectrum of Cy5-labeled F_1 (*curve 3*) revealed a spectral overlap between donor emission and acceptor absorption (*curves 2* and *3*), which is sufficient for FRET. Specific excitation of the FRET donor at 532 nm resulted in a fluorescence emission of the donor (maximum at 579 nm) and acceptor (the fluorescence emission spectrum of Cy5-labeled F_1 shows the maximum at 670 nm). The efficiency of energy transfer between the fluorophores was clearly not affected by the subunit composition of F_0.

In initial ensemble FRET measurements, reconstituted TMR-labeled F_0 was titrated with increasing concentrations of Cy5-labeled F_1. At low F_1 concentrations, no significant decrease in donor intensity or corresponding increase in acceptor intensity could be observed (data not shown). At high F_1 concentrations, a slight decrease in donor intensity and an increase in acceptor intensity were found due to F_1 binding. However, in this titration experiment, especially in the case of low F_1 concentrations, the acceptor intensity resulted partly from the direct excitation of the acceptor at 532 nm in addition to energy transfer by FRET, thereby covering the signal of interest. Therefore, single-molecule FRET analysis was used to separate the binding events indicated by FRET from the non-binding of F_1 (donor-only events).

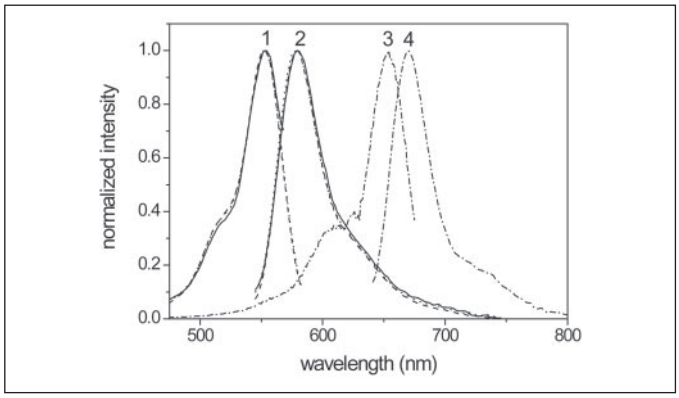

FIGURE 2. **Fluorescence spectra of TMR-labeled F_0 and b_2 and ab_2 subcomplexes reconstituted into liposomes as well as Cy5-labeled F_1.** The excitation spectra (*curves 1*) of proteoliposomes reconstituted from TMR-labeled F_0 (*solid lines*), ab_2 subcomplex (*dashed lines*), and b_2 subcomplex (*dotted lines*) were measured at an emission wavelength of 600 nm, and the emission spectra (*curves 2*) were measured at an excitation wavelength of 532 nm. The excitation spectrum of Cy5-labeled F_1 (*curve 3*) was measured at an emission wavelength 670 nm, and the emission spectrum (*curve 4*) was measured at an excitation wavelength of 600 nm.

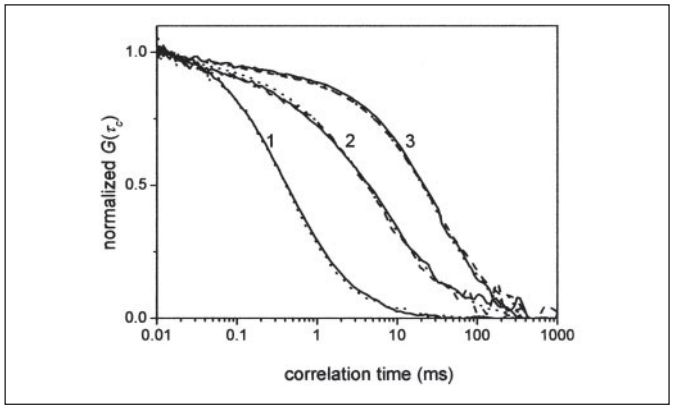

FIGURE 3. **Normalized fluorescence autocorrelation functions of TMR and TMR-labeled F_0 and ab_2 and b_2 subcomplexes.** Autocorrelation functions ($G(\tau_c)$) were normalized at τ_c = 0.01 ms. *Curves 1*, free TMR (*solid line*) and TMR added to liposomes (*dotted line*); *curves 2*, TMR-labeled F_0 (*solid line*), ab_2 subcomplex (*dashed line*), and b_2 subcomplex (*dotted line*) in solution; *curves 3*, TMR-labeled F_0 (*solid line*), ab_2 subcomplex (*dashed line*), and b_2 subcomplex (*dotted line*) reconstituted into liposomes. The data collection time for one curve was 10 s.

Fluorescence Correlation Spectroscopy—In confocal single-molecule spectroscopy, the signature of an individual fluorophore is a burst of photons as the molecule is repeatedly excited while diffusing through the laser focus. To specifically detect the reconstituted F_0 components after binding of F_1, the photon bursts that were caused by freely diffusing labeled protein or dye molecules had to be discriminated from those of the labeled proteoliposomes. The average duration of the photon bursts from single fluorophores, labeled proteins, and labeled proteoliposomes depends on the size of the particle. Therefore, they can be distinguished by their diffusion correlation time (τ_D).

Fig. 3 shows the autocorrelation functions ($G(\tau_c)$) of TMR and TMR-labeled F_0 and ab_2 and b_2 subcomplexes as well as TMR-labeled proteoli-

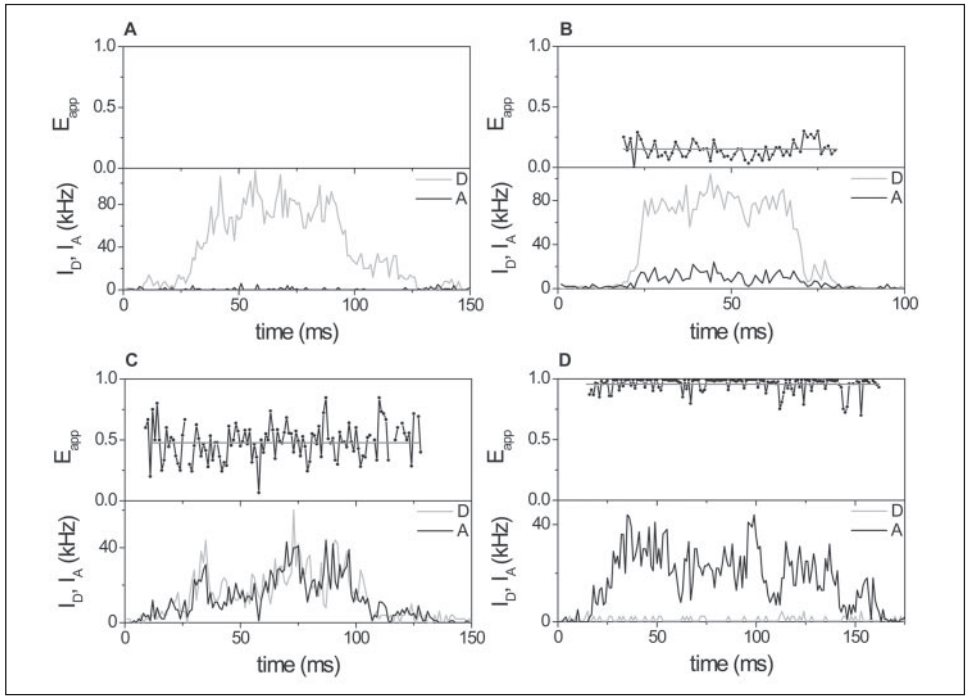

FIGURE 4. **Photon bursts and apparent energy transfer efficiency of FRET signals of single proteoliposomes.** *A*, donor only; *B*, low FRET state; *C*, medium FRET state; *D*, high FRET state. The lower part of each panel represents the time trajectories of TMR fluorescence intensities (I_D, *gray traces*) and Cy5 fluorescence intensities (I_A, *black traces*). The upper part shows the corresponding apparent FRET efficiencies (E_{app}, *black traces*) and the mean FRET efficiency of the burst (*gray lines*).

posomes. Shifts in the autocorrelation functions from shorter to longer correlation times (*i.e.* the shifts from *curves 1* to *curves 2* and to *curves 3*) indicate that the molecules diffused more slowly because of an increasing molecular mass of the diffusing particle. For free TMR, a diffusion time of 0.42 ms was obtained (*curves 1*). The same diffusion time was measured in the presence of unlabeled liposomes, thereby indicating that there was no unspecific binding of TMR to the liposomes. Surprisingly, for TMR-labeled F_0 as well as the ab_2 subcomplex and subunit *b* in detergent-containing buffer solutions, similar values of $\tau_D = 5.7$ ms were obtained in all three cases (*curves 2*). The diffusion time should increase with the radius of the diffusing particle; thus, the diffusion time is expected to increase with the molecular mass. In contrast to the expected values, equal diffusion times were found for subunit *b*, the ab_2 subcomplex, and F_0. This is presumably due to the fact that the hydrophobic parts of these proteins are surrounded by detergent micelles. This results in an increase in the radius of the different particles, so they have almost similar hydrodynamic radii. Accordingly, equal diffusion times of 24 ms were also found for proteoliposomes with TMR-labeled F_0, ab_2 subcomplex, or subunit *b* (*curves 3*). As expected, the diffusion times observed for proteoliposome samples were independent of the incorporated F_0 components because the diffusion time was dominated by the large volume of the liposomes. An almost identical diffusion time of 25 ms was found for the liposomes, in which the TMR was covalently attached to the lipids (data not shown). The differences between the determined diffusion times of freely diffusing and reconstituted proteins were large enough to provide the selection criteria for the single-molecule FRET titration experiments.

Single-molecule FRET Titrations—Single-molecule spectroscopy allowed us to distinguish between liposomes reconstituted with TMR-labeled F_0, ab_2 subcomplex, and subunit *b* (donor-only event) and TMR-labeled proteoliposomes with bound Cy5-labeled F_1 (FRET event). Proteoliposomes were titrated with increasing concentrations of F_1 to measure the differential binding of F_1 to the different complexes.

Cy5-labeled F_1 was excited to a small extent at the wavelength used for the excitation of TMR, thereby complicating the distinction between photon bursts obtained from donor-only and FRET events at high F_1 concentrations. Therefore, unbound F_1 was separated from the proteoliposome samples by centrifugation after binding equilibrium was reached and before the relative number of FRET events was measured. The assumption that the equilibrium was "frozen" (equilibrium is established so slowly that it does not change during the measurements) was checked in two ways. At low concentrations, the effect of direct excitation of Cy5-labeled F_1 did not prevent the distinction of FRET and donor-only events. Similar results were obtained when free F_1 had been separated from the proteoliposome samples by centrifugation. However, at high concentrations, the separation of free F_1 was necessary. Under these conditions, the relative number of FRET events was analyzed at the beginning and end of the measurements, but no significant difference was detected. Accordingly, there was no shift in equilibrium within the time range of the measurement (30 min).

After removal of unbound F_1, the samples were diluted to a concentration of 100 pM, and photon bursts resulting from proteoliposomes were analyzed under a confocal microscope with two-channel detection. Well separated long-lasting photon bursts could be observed for all samples (Fig. 4). For each photon burst, the apparent FRET efficiencies (E_{app}) were calculated as time trajectories (E_{app}, *black traces*) using $E_{app} = I_A/(I_D + I_A)$ from the corrected fluorescence intensities of the donor TMR (I_D, *gray traces*) and the acceptor Cy5 (I_A, *black traces*). Photon bursts were classified according to their mean FRET efficiency into donor-only events with $E_{app} \leq 0.05$ or FRET events with $E_{app} > 0.05$. Fig. 4*A* shows a typical photon burst of a donor-only event, where the fluorescence intensity in the acceptor channel is at the background level. This could result from the following. 1) No binding of F_1 occurred. Consequently, the proteoliposomes contained only the donor fluorophore at subunit *b*. 2) Binding of unlabeled F_1 molecule occurred. Only 58% of F_1 was labeled with Cy5; and thus, 42% of the photon bursts lacked the acceptor. 3) Binding of Cy5-labeled F_1 occurred, but photobleaching of the Cy5 dye prior to detection resulted in a donor-only event. The observed FRET events were found to be subdivided into three different FRET efficiency states: a low FRET state (Fig. 4*B*), a medium FRET state (Fig. 4*C*), and a high FRET state (Fig. 4*D*). These three FRET states could be attributed to the three different distances between the donor at subunit *b* and the acceptor at the γ subunit corresponding to the three possible orientations of the γ subunit in F_1F_0 with respect to the subunit *b* dimer as reported previously (7, 29).

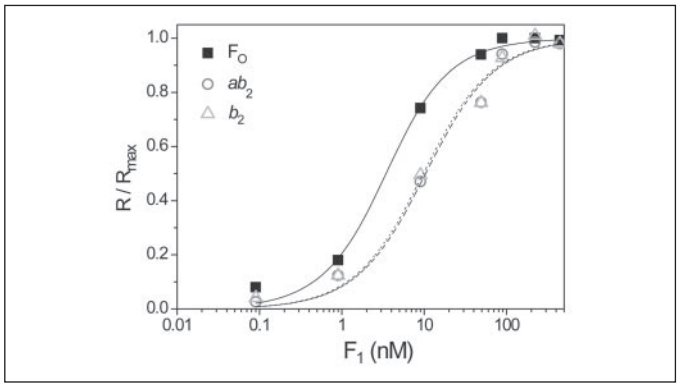

FIGURE 5. **Binding of Cy5-labeled F_1 to TMR-labeled F_0 and ab_2 and b_2 subcomplexes observed by single-molecule FRET.** The relative number of FRET events (R/R_{max}) is plotted against the initial F_1 concentration. ■——■, F_0; ○– – –○, ab_2 subcomplex; △…△, b_2 subcomplex. The curves were calculated according to Equation 3.

The binding of F_1 to reconstituted F_0 can be described by the dissociation constant of F_1F_0, K_d (Equation 2),

$$F_1F_0 \leftrightarrows F_1 + F_0, \qquad K_d = \frac{[F_0][F_1]}{[F_1F_0]} \qquad \text{(Eq. 2)}$$

where $[F_0]$, $[F_1]$, and $[F_1F_0]$ represent the concentrations at equilibrium. For each F_0 component and particular F_1 concentration, 200–300 photon bursts were analyzed, and the total number of events and the number of events showing intramolecular FRET were counted one by one. Generally, a higher number of FRET events could be observed with increasing F_1 concentrations, reaching constant maximum values at $[F_1] > 80$ nM. The ratio of FRET events to all events (R) was calculated for the different F_1 concentrations used. For the titration of F_0 with F_1, R reached the maximum value (R_{max}) of 50% at an initial F_1 concentration of 89 nM. In contrast, to reach the corresponding R_{max} values of 50% for the ab_2 subcomplex and 49% for the subunit b dimer, a significantly higher F_1 concentration of 222 nM was required. The changes in the relative number of FRET events (R/R_{max}) were plotted for 15 nM reconstituted F_0, ab_2 subcomplex, and subunit b as a function of the initial F_1 concentration (Fig. 5). To obtain the corresponding binding constants, the specific relations of R/R_{max} and the initial concentrations were derived as deduced in the "Appendix." The K_d for the binding of F_1 to F_0 and respective components was calculated according to Equation 3,

$$\frac{R}{R_{max}} = \frac{[F_1F_0]}{[F_0]_0} = \frac{1}{2[F_0]_0} \cdot \{K_d + [F_1]_0 + [F_0]_0 \pm ((-K_d - [F_1]_0 - [F_0]_0)^2 - 4[F_0]_0[F_1]_0)^{1/2}\} \qquad \text{(Eq. 3)}$$

where $[F_1F_0]$ is the concentration of F_1F_0 at equilibrium and $[F_0]_0$ and $[F_1]_0$ are the starting concentrations of F_0 and F_1, respectively, at the beginning of the titration. The same equation holds for the ab_2 and b_2 subcomplexes if $[F_0]_0$ is substituted with $[ab_2]_0$ or $[b_2]_0$, respectively. Equation 3 is deduced in the "Appendix."

In Fig. 5, the curves were calculated according to Equation 3, and the dissociation constant (K_d) was obtained from a nonlinear fit to the data. This results in $K_d = 2.7 \pm 0.7$ nM for F_0, $K_d = 9.7 \pm 1.2$ nM for the ab_2 subcomplex, and $K_d = 9.0 \pm 1.3$ nM for the subunit b dimer. The dissociation constants for the reconstituted ab_2 subcomplex and subunit b are the same within error limits. This might indicate that subunit a does not contribute to the binding of F_1. However, in addition to the subunit b dimer, the presence of the subunit c ring in assembled F_0 complexes is necessary for high affinity binding of F_1.

DISCUSSION

According to the current model of rotational catalysis within F_1F_0-ATP synthase in conjunction with the hypothesis of elastic coupling between proton translocation in F_0 and ATP turnover in F_1, both the rotor and stator are supposed to withstand a rotary strain of ~55 kJ mol^{-1} (19, 20). Thus, strong interactions of subunits involved in rotor and stator formation are required. In this context, it is generally noteworthy that, for binding assays, the binding affinities of subunits do not necessarily have to reflect the interaction energy of subunits or torque values within an operating enzyme because the directions of the force vectors are most probably not identical.

Binding affinities have been determined in solution for subunits of the peripheral stator (*i.e.* subunits b and δ) (20, 22, 46). However, subunit interactions within the rotor part have not yet been considered for their substantial contribution to the binding of F_1 to F_0, which has, however, been demonstrated by functional reconstitution of F_0 and subcomplexes thereof (23, 27). In solution, the binding strength of the isolated subunit b dimer with F_1 is thought to be at least in part equivalent to the torque, which is built up during catalysis (22). However, in the experiments performed so far, only a simple docking of subunits could be observed, which did not result in the formation of functional enzyme complexes because of the lack of the other F_0 subunits. Furthermore, the use of truncated forms of subunit b lacking the membrane part confused the interpretation of the data obtained with only a weak tendency to form dimers in solution. Dimerization constants in the range of 1–2 μM have been revealed to be in conflict with the determination of the binding affinities of the subunit b dimer for F_1 in the nanomolar range (20). It has previously been shown that the two b subunits also interact via their transmembrane regions (26), thereby obviously contributing to the dimerization of the polypeptide.

To analyze the binding affinity of F_1 for F_0 and subcomplexes thereof via the subunit b dimer under "*in vivo*" conditions, it was necessary to combine functional reconstitution and quantitative spectroscopic analysis of subunit interactions. Based on fully assembled F_0, this approach provides for the first time the possibility to study the contribution of each F_0 subunit to the F_1 interaction. Also the problem of a low dimerization constant was overcome by use of reconstituted subunit b because, at least within the ab_2 subcomplex, the two b subunits are assembled as a dimer. From our results, it becomes evident that the same is true for reconstituted subunit b because its K_d is identical to the ab_2 subcomplex K_d. In contrast to all other corresponding experiments performed so far, in this study, functional F_1F_0 interactions were observed because the presence of the label did not interfere with the ATPase activity of the resulting enzymes and did not affect the ability of F_1F_0 to synthesize ATP.

Initial experiments with molecule ensembles indicated FRET after binding of F_1 to F_0. The labeling efficiency of the FRET acceptor at F_1 was 58%, which limited the maximum fluorescence changes to be achieved by FRET. At low F_1 concentrations, only a small decrease on FRET donor fluorescence indicated the binding events. In addition, three distances with different FRET efficiencies were expected between the donor at bCys^{64} and the acceptor at the γ subunit according to the three possible γ subunit orientations within F_1 (7, 29). However, it was not possible to quantitatively attribute the increase in acceptor fluorescence at ~670 nm to FRET as a result of the binding event because there was an increasing error due to the direct excitation of the acceptor with increasing concentrations of Cy5-labeled F_1 (without binding to F_0 or the subcomplexes). Therefore, single-molecule FRET analysis was the method of choice. In these titration experiments, defined incubation conditions were employed. The background fluorescence in the acceptor channel was suppressed by separating the proteoliposomes from unbound F_1 by ultracentrifugation. F_1 was thereby removed from the equilibrium. How-

ever, subsequent dissociation of F_1 was not observed during the time of measurement, indicating only very small dissociation rates for bound F_1.

Single F_0 or subcomplexes reconstituted into liposomes were counted one after another, and FRET within the photon bursts characterized the binding of F_1. By analyzing several hundred single proteoliposomes, even small numbers of FRET events were unambiguously identified, resulting in a high reproducibility of the number of FRET and donor-only events. The FRET acceptor labeling degree of 58% represents the theoretical upper limit for the relative number of FRET events, when every donor-labeled F_0, ab_2 subcomplex, or subunit *b* dimer has bound F_1. The experimental value of 50% for R_{max} indicates that photobleaching of the FRET acceptor was marginal. The difference from the theoretical value could be due to a small fraction of F_1 lacking either the δ or ϵ subunit, which prevents binding of F_1 to the different proteoliposomes.

The K_d values derived from these single-molecule FRET data clearly demonstrate that subunit *b* (not as a dimer or assembled in ab_2 subcomplexes) is solely responsible for efficient F_1 binding. This is in accord with former functional reconstitution experiments (23, 27). Only in the case of fully assembled F_0 complexes was a K_d of 2.7 nM observed, matching a magnitude of ~50 kJ mol^{-1}, which can be considered to be almost sufficient to withstand the rotary strain within the stator during catalysis. Both the subunit *b* dimer and ab_2 subcomplex showed significantly lower but identical K_d values. From this, it can be additionally concluded that subunit *a* does not substantially contribute to F_1 binding (not by direct interactions or via a possible influence on the subunit *b* dimer). The additional presence of the subunit *c* ring decreases the dissociation constant of F_1 by ~3-fold. Hence, interactions of the proteolipid ring with rotor components of F_1 are also involved in binding within the assembled enzyme. Protein contacts of the hydrophilic loop domain of subunit *c* with the γ and ϵ subunits were shown by chemical cross-linking (47–50). The binding strength of subunits within the rotor part should be at least equal to that within the stator of the enzyme. Because F_1 and F_0 each contain components of both the rotor and stator, corresponding contributions of subunit interactions are also expected to occur within the $\gamma\epsilon c_{10}$ rotor.

However, the differences in the F_1 binding affinities, which were determined to be 2.7 nM for F_0 and 9.0 and 9.7 nM for the subunit *b* dimer and ab_2 subcomplex, respectively, are significant; and, furthermore, these values were obtained within the same analytical setup, thus providing a direct comparability of the samples. Subunit interactions within the stator part of F_1F_0 were so far determined with different methods and experimental techniques, including FCS analysis (20, 46) and tryptophan fluorescence measurements (22, 51), thereby rendering the comparison of the data obtained rather difficult. In addition, the use of unassembled or truncated subunits in these previous studies did not allow the detection of possible cooperative binding effects of more than one polypeptide. This may explain the rather broad range of dissociation constants found for stator subunit interactions, ranging from 1–2 nM (46, 51) to 5–10 μM (21). The maximum binding energy of 48.9 kJ mol^{-1}, which was calculated in our study, apparently does not reflect the maximum ΔG value of ATP synthesis, which is reported to be 55 kJ mol^{-1} (19, 20). Several models for the calculation of binding constants also accounting for a possible additional or cooperative contribution of the δ subunit to F_1 binding did not result in significantly higher ΔG values. This clearly argues again for the fact that the direction of the force vectors for F_1 binding and rotation are not identical. However, it should be noted that these apparent binding energies of 48.9 kJ mol^{-1} for F_0 *versus* 45.9/45.7 kJ mol^{-1} for the subunit *b* and ab_2 subcomplex, respectively, represent the lower limits. Dissociation of the δ subunit in F_1, which has been reported to occur with a K_d of ~1 nM (46, 51), as well as possible partial loss of the ϵ subunit could reduce the effective fraction of functional F_1 in the FRET titration experiments, resulting in higher binding energies and correspondingly lower K_d values. To obtain an estimation of this effect, one can assume that the effective concentration of F_1 ($[F_1]_0$) is only 50% of the stoichiometric value. In this case, the K_d for the F_1/F_0 interaction changes from 2.7 to 1.1 nM. The effective F_0 concentration was determined with the two-parameter fit of the F_0 titration data, resulting in $[F_0]_0$ = 1.5 nM. The stoichiometric concentration determined by protein concentration assays is 15 nM, indicating that the effective fraction of F_0 in the sample, *i.e.* the concentration of F_0 that is able to bind F_1, is drastically reduced. This is also reflected by a comparatively large fraction of impurities in the F_0 preparation. In contrast to $[F_1]_0$, a higher $[F_0]_0$ value would lead to lower K_d values.

However, from the differences in the calculated binding energies, it can be concluded that the interaction of the subunit *b* dimer with F_1 makes up for the main fraction in binding affinity. This is in good accord with cross-linking data, from which extensive protein contact sites of subunit *b* with subunits of F_1 can be derived (17). In contrast, F_1/F_0 interactions within the rotor part of the enzyme are restricted to the polar loop region of the subunit *c* ring (49), which explains the small but still essential contribution of the proteolipid to F_1 binding.

APPENDIX

The binding of F_1 to reconstituted F_0 can be described by the dissociation constant of F_1F_0, K_d, as in Equation 2 under "Results."

From the mass balance for F_0, the concentrations of F_0 and F_1 at equilibrium are obtained (Equations 4 and 5),

$$[F_0] = [F_0]_0 - [F_1F_0] \quad \text{(Eq. 4)}$$

$$[F_1] = [F_1]_0 - [F_1F_0] \quad \text{(Eq. 5)}$$

where $[F_0]$, $[F_1]$, and $[F_1F_0]$ are the free concentrations at equilibrium and $[F_0]_0$ and $[F_1]_0$ are the initially added concentrations.

Combining Equations 2, 4, and 5 yields Equation 6.

$$K_d = \frac{([F_0]_0 - [F_1F_0])([F_1]_0 - [F_1F_0])}{[F_1F_0]} \quad \text{(Eq. 6)}$$

Rearrangement of Equation 6 gives Equation 7.

$$[F_1F_0] = \frac{1}{2}\{(K_d + [F_1]_0 + [F_0]_0) \pm ((-K_d - [F_1]_0 - [F_0]_0)^2 - 4[F_0]_0[F_1]_0)^{1/2}\} \quad \text{(Eq. 7)}$$

At a constant initial F_0 concentration of 15 nM, different initial F_1 concentrations were added. Photon bursts for each concentration were measured, and the number of bursts indicating FRET events ($N_{(DA)}$) and the number of photon bursts without FRET (donor-only event; $N_{(DO)}$) were counted.

The number of FRET events is proportional to the concentration of double-labeled F_1F_0 ($F_0^{TMR}F_1^{Cy5}$) (Equation 8),

$$N_{(DA)} \sim [F_0^{TMR}F_1^{Cy5}] \quad \text{(Eq. 8)}$$

where $N_{initial(DA)} = 0$ before the addition of F_1.

At the highest concentration of titrated F_1 suggesting complete binding of F_1 to F_0, the maximum number of FRET events ($N_{max(DA)}$) is obtained (Equation 9),

$$N_{max(DA)} \sim [F_0^{TMR}F_1^{Cy5}]_{max} = \alpha[F_0^{TMR}]_0 = \alpha\beta[F_0]_0 \quad \text{(Eq. 9)}$$

where α reflects the degree of Cy5 labeling of F_1 ($[F_1^{Cy5}] = \alpha[F_1]_0$) and β reflects the degree of TMR labeling of F_0 ($[F_0^{TMR}]_0 = \beta[F_0]_0$).

The number of donor-only events is proportional to the concentrations of F_0^{TMR} and $F_0^{TMR}F_1$ (Equation 10).

$$N_{(DO)} \sim ([F_0^{TMR}] + [F_0^{TMR}F_1]) \quad \text{(Eq. 10)}$$

At the maximum F_1 concentration, we obtain Equation 11,

$$N_{max(DO)} \sim [F_0^{TMR}F_1] = \beta(1-\alpha)[F_0]_0 \quad \text{(Eq. 11)}$$

where $1-\alpha$ is the fraction of unlabeled F_1.

The ratio of the number of FRET events to the total number of events is calculated by combining Equations 8 and 10 (Equation 12).

$$R = \frac{N_{(DA)}}{N_{(DA)} + N_{(DO)}} = \frac{[F_0^{TMR}F_1^{Cy5}]}{[F_0^{TMR}F_1^{Cy5}] + [F_0^{TMR}] + [F_0^{TMR}F_1]} = \frac{\alpha\beta[F_1F_0]}{\beta[F_0]_0} = \frac{\alpha[F_1F_0]}{[F_0]_0} \quad \text{(Eq. 12)}$$

Accordingly, the maximum ratio (R_{max}) is obtained from Equations 9 and 11 (Equation 13),

$$R_{max} = \frac{N_{max(DA)}}{N_{max(DA)} + N_{max(DO)}} = \frac{\alpha\beta[F_0]_0}{\alpha\beta[F_0]_0 + \beta(1-\alpha)[F_0]_0} = \alpha \quad \text{(Eq. 13)}$$

which equals the degree of labeling (α) of F_1.

Combining Equations 12 and 13 results in the relative number of FRET events, R/R_{max} (Equation 14).

$$\frac{R}{R_{max}} = \frac{\alpha[F_1F_0]}{[F_0]_0\alpha} = \frac{[F_1F_0]}{[F_0]_0} \quad \text{(Eq. 14)}$$

From Equations 7 and 14, the relation between the relative number of FRET events and the dissociation constant is finally obtained, as in Equation 3 under "Results."

Acknowledgment—We thank N. Zarrabi (Universität Stuttgart) for providing the software Burst Analyzer.

REFERENCES

1. Weber, J., and Senior, A. E. (2003) *FEBS Lett.* **545,** 61–70
2. Fillingame, R. H., and Dmitriev, O. Y. (2002) *Biochim. Biophys. Acta* **1565,** 232–245
3. Zhou, Y., Duncan, T. M., and Cross, R. L. (1997) *Proc. Natl. Acad. Sci. U. S. A.* **94,** 10583–10587
4. Noji, H., Yasuda, R., Yoshida, M., and Kinosita, K., Jr. (1997) *Nature* **386,** 299–302
5. Junge, W. (1999) *Proc. Natl. Acad. Sci. U. S. A.* **96,** 4735–4737
6. Yasuda, R., Noji, H., Yoshida, M., Kinosita, K., Jr., and Itoh, H. (2001) *Nature* **410,** 898–904
7. Diez, M., Zimmermann, B., Börsch, M., König, M., Schweinberger, E., Steigmiller, S., Reuter, R., Felekyan, S., Kudryavtsev, V., Seidel, C. A., and Gräber, P. (2004) *Nat. Struct. Mol. Biol.* **11,** 135–141
8. Zimmermann, B., Diez, M., Nawid, Z., Gräber, P., and Börsch, M. (2005) *EMBO J.,* **24,** 2053–2063
9. Wilkens, S., and Capaldi, R. A. (1998) *Nature* **393,** 29
10. McLachlin, D. T., Coveny, A. M., Clark, S. M., and Dunn, S. D. (2000) *J. Biol. Chem.* **275,** 17571–17577
11. Greie, J.-C., Deckers-Hebestreit, G., and Altendorf, K. (2000) *Eur. J. Biochem.* **267,** 3040–3048
12. Altendorf, K., Stalz, W.-D., Greie, J.-C., and Deckers-Hebestreit, G. (2000) *J. Exp. Biol.* **203,** 19–28
13. Meier, T., Polzer, P., Diederichs, K., Welte, W., and Dimroth, P. (2005) *Science* **308,** 659–662
14. Dunn, S. D., Revington, M., Cipriano, D. J., and Shilton, B. H. (2000) *J. Bioenerg. Biomembr.* **32,** 347–355
15. McLachlin, D. T., and Dunn, S. D. (2000) *Biochemistry* **39,** 3486–3490
16. Fillingame, R. H., Jiang, W., Dmitriev, O. Y., and Jones, P. C. (2000) *Biochim. Biophys. Acta* **1458,** 387–403
17. Greie, J.-C., Deckers-Hebestreit, G., and Altendorf, K. (2000) *J. Bioenerg. Biomembr.* **32,** 357–364
18. Long, J. C., DeLeon-Rangel, J., and Vik, S. B. (2002) *J. Biol. Chem.* **277,** 27288–27293
19. Pänke, O., Cherepanov, D. A., Gumbiowski, K., Engelbrecht, S., and Junge, W. (2001) *Biophys. J.* **81,** 1220–1233
20. Diez, M., Börsch, M., Zimmermann, B., Turina, P., Dunn, S. D., and Gräber, P. (2004) *Biochemistry* **43,** 1054–1064
21. Dunn, S. D., and Chandler, J. (1998) *J. Biol. Chem.* **273,** 8646–8651
22. Weber, J., Wilke-Mounts, S., Nadanaciva, S., and Senior, A. E. (2004) *J. Biol. Chem.* **279,** 11253–11258
23. Stalz, W.-D., Greie, J.-C., Deckers-Hebestreit, G., and Altendorf, K. (2003) *J. Biol. Chem.* **278,** 27068–27071
24. Weber, J., Muharemagic, A., Wilke-Mounts, S., and Senior, A. E. (2003) *J. Biol. Chem.* **278,** 13623–13626
25. Dunn, S. D. (1992) *J. Biol. Chem.* **267,** 7630–7636
26. Dmitriev, O., Jones, P. C., Jiang, W., and Fillingame, R. H. (1999) *J. Biol. Chem.* **274,** 15598–15604
27. Greie, J.-C., Heitkamp, T., and Altendorf, K. (2004) *Eur. J. Biochem.* **271,** 3036–3042
28. Kauffer, S., Deckers-Hebestreit, G., and Altendorf, K. (1991) *Eur. J. Biochem.* **202,** 1307–1312
29. Börsch, M., Diez, M., Zimmermann, B., Reuter, R., and Gräber, P. (2002) *FEBS Lett.* **527,** 147–152
30. Iwamoto, A., Omote, H., Hanada, H., Tomioka, N., Itai, A., Maeda, M., and Futai, M. (1991) *J. Biol. Chem.* **266,** 16350–16355
31. Ho, S. N., Hunt, H. D., Horton, R. M., Pullen, J. K., and Pease, L. R. (1989) *Gene* (*Amst.*) **77,** 51–59
32. Klionsky, D. J., Brusilow, W. S., and Simoni, R. D. (1984) *J. Bacteriol.* **160,** 1055–1060
33. Gogol, E. P., Lücken, U., Bork, T., and Capaldi, R. A. (1989) *Biochemistry* **28,** 4709–4716
34. Aggeler, R., and Capaldi, R. A. (1992) *J. Biol. Chem.* **267,** 21355–21359
35. Schneider, E., and Altendorf, K. (1984) *Proc. Natl. Acad. Sci. U. S. A.* **81,** 7279–7283
36. Börsch, M., Turina, P., Eggeling, C., Fries, J. R., Seidel, C. A., Labahn, A., and Gräber, P. (1998) *FEBS Lett.* **437,** 251–254
37. Fischer, S., and Gräber, P. (1999) *FEBS Lett.* **457,** 327–332
38. Fischer, S., Etzold, C., Turina, P., Deckers-Hebestreit, G., Altendorf, K., and Gräber, P. (1994) *Eur. J. Biochem.* **225,** 167–172
39. Gill, S. C., and von Hippel, P. H. (1989) *Anal. Biochem.* **182,** 319–326
40. Schägger, H., and von Jagow, G. (1987) *Anal. Biochem.* **166,** 368–379
41. Blum, H., Beier, H., and Gross, H. J. (1987) *Electrophoresis* **8,** 93–99
42. Fischer, S., Gräber, P., and Turina, P. (2000) *J. Biol. Chem.* **275,** 30157–30162
43. Turina, P., Samoray, D., and Gräber, P. (2003) *EMBO J.* **22,** 418–426
44. Rodgers, A. J., Wilkens, S., Aggeler, R., Morris, M. B., Howitt, S. M., and Capaldi, R. A. (1997) *J. Biol. Chem.* **272,** 31058–31064
45. Förster, T. (1948) *Ann. Phys.* **2,** 55–70
46. Häsler, K., Pänke, O., and Junge, W. (1999) *Biochemistry* **38,** 13759–13765
47. Watts, S. D., Zhang, Y., Fillingame, R. H., and Capaldi, R. A. (1995) *FEBS Lett.* **368,** 235–238
48. Watts, S. D., Tang, C., and Capaldi, R. A. (1996) *J. Biol. Chem.* **271,** 28341–28347
49. Hermolin, J., Dmitriev, O. Y., Zhang, Y., and Fillingame, R. H. (1999) *J. Biol. Chem.* **274,** 17011–17016
50. Bulygin, V. V., Duncan, T. M., and Cross, R. L. (2004) *J. Biol. Chem.* **279,** 35616–35621
51. Weber, J., Wilke-Mounts, S., and Senior, A. E. (2002) *J. Biol. Chem.* **277,** 18390–18396